Accepted Manuscript

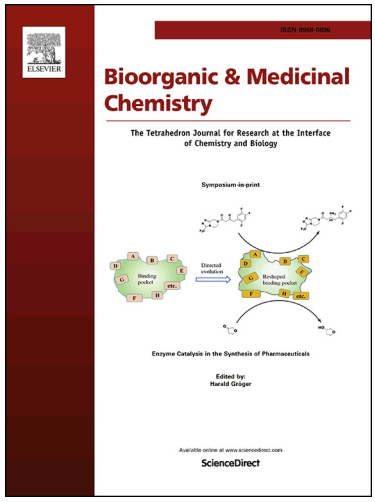

Inhibition of the FAD containing ER oxidoreductin 1 (Ero1) protein by EN-460 a strategy for treatment of multiple myeloma

Karen Hayes, Paratchata Batsomboon, Wei-Chih Chen, Andreas Becker, Steven Escherich, Yan Yang, Aaron R. Robart, Gregory Dudley, Werner J. Geldenhuys, Lori A Hazlehurst

PII: S0968-0896(18)31885-6
DOI: https://doi.org/10.1016/j.bmc.2019.02.016
Reference: BMC 14752

To appear in: *Bioorganic & Medicinal Chemistry*

Received Date: 21 November 2018
Revised Date: 31 January 2019
Accepted Date: 8 February 2019

Please cite this article as: Hayes, K., Batsomboon, P., Chen, W-C., Becker, A., Escherich, S., Yang, Y., Robart, A.R., Dudley, G., Geldenhuys, W.J., Hazlehurst, L.A., Inhibition of the FAD containing ER oxidoreductin 1 (Ero1) protein by EN-460 a strategy for treatment of multiple myeloma, *Bioorganic & Medicinal Chemistry* (2019), doi: https://doi.org/10.1016/j.bmc.2019.02.016

For Bioorg Med Chem

Inhibition of the FAD containing ER oxidoreductin 1 (Ero1) protein by EN-460 a strategy for treatment of multiple myeloma

Karen Hayes,[1] Paratchata Batsomboon,[2] Wei-Chih Chen,[1] Andreas Becker,[3] Steven Escherich,[3] Yan Yang,[3] Aaron R. Robart,[4] Gregory Dudley,[2,5] Werner J. Geldenhuys,[1,2,5,6*] and Lori A Hazlehurst[1,5*]

[1]*Pharmaceutical Sciences, School of Pharmacy, West Virginia University, Morganton WV, 26506*

[2] *C. Eugene Bennett Department of Chemistry, West Virginia University, Morgantown, WV 26506*

[3]*Moffitt Cancer Center, Tampa Florida 33612*

[4]*Biochemistry, School of Medicine, West Virginia University, Morgantown, WV, 26506*

[5]*Cancer Center, West Virginia University, Morgantown, WV, 26506*

[6]*Department of Neuroscience, School of Medicine, West Virginia University, Morgantown, WV, 26506*

Corresponding Authors: 1 Medical Center Drive, Morgantown WV 26506 USA; Email: lahazlehurst@hsc.wvu.edu; Werner.geldenhuys@hsc.wvu.edu

Abstract

Multiple myeloma (MM) cells demonstrate high basal endoplasmic reticulum (ER) stress and are typically exquisitely sensitive to agents such as proteasome inhibitors that activate the unfolded protein response. The flavin adenosine dinucleotide (FAD) containing endoplasmic reticulum oxidoreductin enzyme (Ero1L) catalyzes de-novo disulfide bridge formation of ER resident proteins and contributes to proper protein folding. Here we show that increased Ero1L expression is a prognostic of poor outcomes for MM patients relapsing on therapy. We propose that targeting protein folding via inhibition of Ero1L may represent a novel therapeutic strategy for the treatment of MM. In this report we show that treatment of MM cells with EN-460, a known inhibitor of ERO1L, was sufficient to inhibit cell proliferation and induce apoptosis. Furthermore, we show that cell death correlated in part with induction of ER stress. We also show that EN460 inhibited the enzyme activity of Ero1L, with an IC50 of 22.13 μM, consistent with previous reports. However, EN-460 was also found to inhibit other FAD-containing enzymes including MAO-A (IC_{50}=7.91 μM), MAO-B (IC_{50}= 30.59 μM) and LSD1 (IC_{50}=4.16 μM), suggesting overlap in inhibitor activity and the potential need to develop more specific inhibitors to enable pharmacological validation of ERO1L as a target for the treatment of MM. We additionally prepared and characterized azide-tagged derivatives of EN-460 as possible functional probe compounds (e.g., for photo-affinity labeling) for future target-engagement studies and further development of structure-activity relationships.

Key words: unfolded protein response; oxidative stress; flavin adenosine dinucleotide

Introduction

Multiple myeloma (MM) is a cancer of plasma cells that home to the bone marrow. Due to the highly secretory function of plasma cells, MM cells are susceptible to high levels of ER stress. In fact, MM cells are uniquely sensitive to proteasome inhibitors and these agents remain a mainstay of clinical treatment[1-4]. Although MM patients will initially respond to proteasome inhibitors all patients relapse with resistant disease[5, 6]. Thus clinical data continue to indicate that additional targets and therapeutic strategies are required to improve MM patient outcomes. Recently, other groups have suggested that exploitation of the ER stress response can be targeted as a mechanism to induce apoptosis in MM cells, by inhibition protein disulphide isomerase (PDI).[7, 8] Moreover, blocking the proteasome with compounds such as velcade has become standard of care for the treatment of MM.[9] Thus the clinical data indicate that inhibition of targets predicted to induce ER stress is a tractable strategy for the treatment of MM

In this study, we focused on the he endoplasmic reticulum (ER) oxidoreductin Ero1L alpha, as one of two proteins that contributes to the formation of disulfide bonds in proteins processed by the ER. Ero1L forms de-novo disulfide bonds and the direct downstream target is PDI. In contract, PDI functions to oxidize downstream target proteins via the formation of disulfide bonds (S-S) during the post-translational modification stage of protein processing in the ER[10]. Ero1L is a Flavin adenosine dinucleotide (FAD) containing enzyme, where FAD is tightly associated with the protein, and plays a role in the Ero1 catalysis mechanisms.

The formation of the disulfide bonds by Ero1L consumes oxygen that is used as terminal electron acceptor in the reaction.[11] Recently the group of Blais et al. identified an Ero1L inhibitor during a high throughput screen (HTS). The hit compound EN460 was found to inhibit the reoxidation of the protein enzyme,[12] however, the activity in MM have not been investigated to date. Our focus in the long term is to target Ero1L for the treatment of cancers susceptible to ER stress, and this current study was initiated to explore the effect of this chemical class on MM cell lines.

MATERIALS AND METHODS

Materials

EN460 was purchased from Tocris. Buffer components were purchased from commercial sources and were of molecular biology grade.

Protein Expression and Purification

Human Ero1α (22-468) with hyperactivating triple mutation (C104A, C131A, and C166A) [insert citation: Inaba, et al., EMBO Journal (2010) 29, 3330–334] DNA was synthnesized and subcloned (GeneArt/Invitrogen) into p15TV-L vector (plasmid 26093, Addgene; Cambridge, MA, USA) using NdeI/NotI sites. ERO1α expression in *E. coli* (BL21(DE3)RIL strain; OD 0.7) was induced with isopropyl β-D-1-thiogalactopyranoside (IPTG, 0.1mM) for 20 h at 18° C. Pelleted bacteria was lysed (50 mM Tris, pH 8.1, 300 mM NaCl, 10 µM FAD, , 0.5% Triton X-100) and Ero1α isolated by affinity chromatography using an Ni-NTA column. His-tagged Ero1α protein bound on Ni-NTA column was washed with 50 mM Tris, pH 8.1, 300 mM NaCl, 10 µM FAD, 20 mM imidazaole then eluted with increased imidazaole (240mM) in wash buffer.

Purified Ero1α protein underwent desalting to remove imidazaole then oxidation with potassium ferricyanide (20mM) for 16 h at 4° C. A preparative Superdex 200 column (GE Heathcare Life Sciences, Pittsburgh, PA, USA) was used to obtain a monomeric Ero1α fraction in 50 mM Tris, pH 8.1, 150 mM NaCl, 10 µM FAD. Concentration of purified hEro1α protein was determined with NanoDrop spectrophotometer (Thermo Fisher Scientific, Waltham, MA, USA) at UV 280 nm.

Human PDI (18-479) DNA was synthesized and subcloned (GeneArt/Invitrogen) into p15TV-L vector and expression induced in *E.coli* as described above. Pelleted bacteria was lysed with 50 mM Tris, pH 8.0, 300 mM NaCl, 1 mM TCEP, 1% Triton X-100, 10 mM Imidazole, and DNase (20 ug/mL) for 1 h at 4°C. His-tagged hPDI protein was isolated from lysate with Ni-NTA Agarose (Invitrogen, Carlsbad, CA, USA). His-tagged PDI bound Ni-NTA resin was washed five times with 50 mM Tris, pH 8.0, 300 mM NaCl, 1 mM TCEP, and 20 mM imidazaole and purified hPDI protein was eluted with wash buffer with 250 mM imidazaole. PD-10 Desalting Columns (GE Heathcare Life Sciences) were used to remove high levels of imidazaole. Purified hPDI protein was concentrated and small molecular weight impurities were removed with Amicon Ultra-15 Centrifugal Filter Unit, 10KDa cutoff (EMD Millipore, Burlington, MA, USA) using 50 mM Tris, pH 8.0, 150 mM NaCl, and 1 mM TCEP buffer. The concentration of purified hPDI protein was determined with NanoDrop spectrophotometer (UV 280 nm).

Amplex Red/Ero1α Catalytic Assay

Purified hyperactive human Ero1α (0.0625 mg/mL), HRP (50 µU/uL, EMD Millipore), Amplex Red (25 µM, Invitrogen) were combined with range of concentrations of purified human PDI (0.250 – 0.008 mg/mL) and/or Ero1α inhibitors (EN460 (EMD Millipore), PB-EN-10; 200 – 0.01 µM) in 50 mM sodium phosphate, pH 7.4 in a 384 well black microplate (Corning,

Tewksbury, MA USA). Microplate was incubated for 30 min at 37° C; Cytation 5 Cell Imaging Multi-Mode Reader (Ex 530, Em 590) (BioTek, Winooski, VT, USA) measured fluorescence intensity.

Protein Thermal Shift Assay

To determine the protein stability, a differential scanning fluorimetry (DSF) study was done. SYPRO Orange Protein Gel Stain (1X, Sigma-Aldrich, St. Louis, MO, USA), purified hEro1α or hPDI proteins (0.250 mg/mL), and Ero1α inhibitors (EN460 or PB-En-10; 20 μM) were combined in 50 mM Tris, pH8.0, 150 mM NaCl in MicroAmp optical 96 well reaction plate (Thermo Fisher Scientific). Melt curve reaction was run on Step One Applied Biosystems real-time PCR system (Life Technologies). Fluorescent readings (target setting: ROX) were collected every 1° C from 25° C to 99° C using a continuous ramp rate. Protein Thermal Shift Software v 1.3 (Life Technologies) was used to analyze results. Melting temperatures (Tm) were generated from derivatives of melt curves (Δ Fluorescence/Δ).

FAD enzyme assays

Monoamine oxidase A and B enzymes was purchased from BD Biosciences. Enzyme activity was determined using kynuramine metabolism by MAO-A and MAO-B as previously published. Fluorescence was determined using BioTek Cytation 5 plate reader, 310/380 Ex/Em nm. LSD-1 activity was determined using a kit from Caymen Chemicals according to the manufacturer's specifications.

Molecular Docking Studies

The crystal structure of Ero1 was obtained from the RCSB Protein Data Bank access code: 3AHQ (hyperactive form).[13] The protein structure was prepared for docking studies using

MOE 2018 (www.chemcomp.com) to add missing hydrogens and ionize the amino acid side-chains at pH 7.4. The FAD core structure was used to delineate the binding pocket, followed by an standard induced fit docking protocol, as implemented in the DOCK program in MOE 2018. The top docked poses were evaluated for specific ligand interactions with the protein.

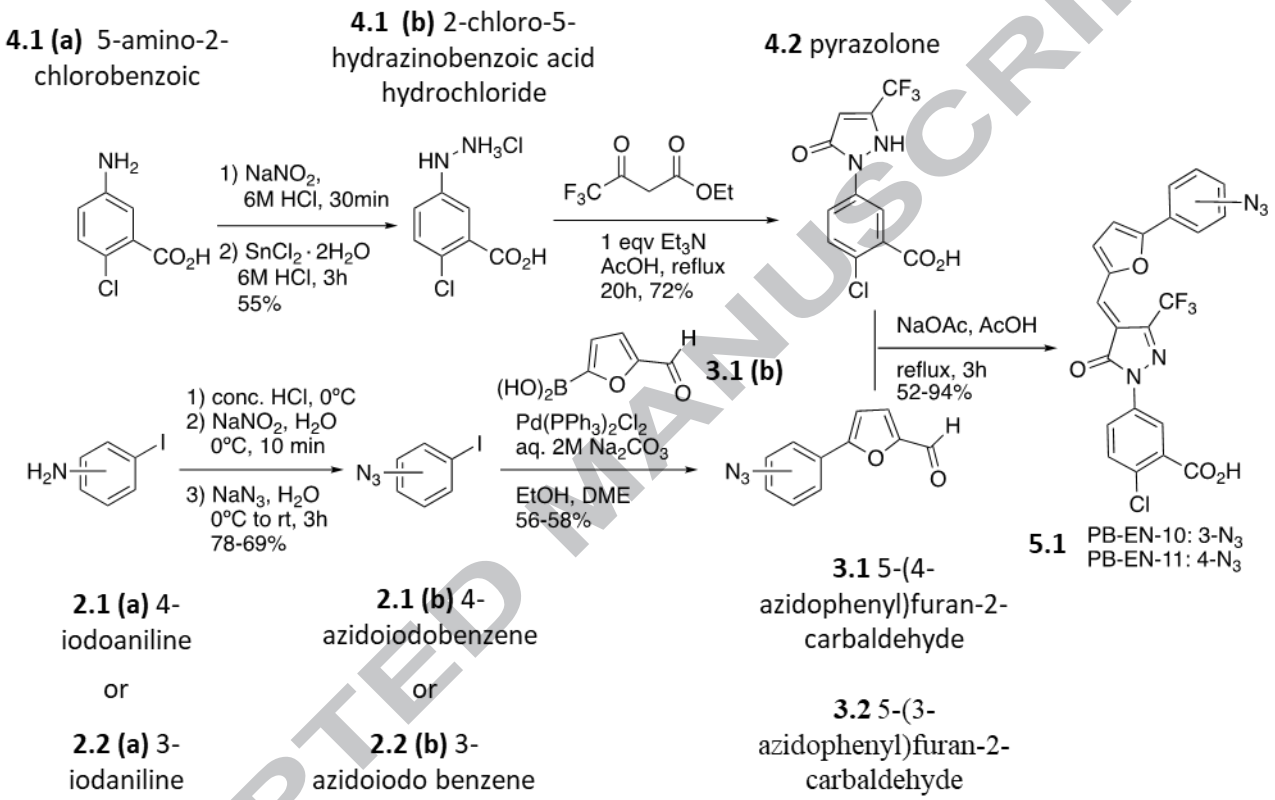

Scheme 1: Synthesis of EN460 derivatives. Pyrazolone (**4.2**) was synthesized as reported previously. (REF: Org. Lett. 2014, 16, 5060−5063) Substituted furfuraldehyes (**3.1** and **3.2**) were synthesized by Suzuki coupling of aryl iodides (**2.1(b)** and **2.2 (b)**) (REF: Org. Lett. 2010, 12, 4217-4219) with furfural-boronic acid (**3.1 (b)**). (REF: Eur. J. Med. Chem. 2017, 126, 929-936) Knoevenagel condensation of the substituted furfuraldehyes (**3.1** and **3.2**) with pyrazolone (**4.2**) using catalytic sodium acetate in acetic acid provided EN460 derivatives PB-10 and PB-11 in 93% and 53% yields, respectively.

The EN460 derivatives were prepared as shown in the Scheme 1. Pyrazolone **3** was synthesized as reported previously.[14] Substituted furfuraldehyes **9** and **10** were synthesized by Suzuki coupling of aryl iodides **6** and **7**[15] with furfural-boronic acid **8**.[16] Knoevenagel condensation of the substituted furfuraldehyes (**9** and **10**) with pyrazolone **3** using catalytic sodium acetate in acetic acid provided EN460 derivatives **PB-10** and **PB-11** in 93% and 53% yields, respectively.

1. Chemistry

All the chemicals were used as received unless otherwise stated. All solvents, solutions and liquid reagents were added via syringe. All reactions were carried out under an inert nitrogen atmosphere unless otherwise stated. The purifications were performed by flash chromatography using silica gel F-254 (230-499 mesh particle size). Yields refer to isolated material judged to be ≥95% pure by ^{1}H NMR spectroscopy following silica gel chromatography. ^{1}H-NMR and ^{13}C-NMR spectra were recorded on a JEOL 400 MHz spectrometer using $CDCl_3$ or DMSO-d_6 as the deuterated solvent. The chemical shifts (δ) are reported in parts per million (ppm) relative to the residual $CHCl_3$ peak (7.26 ppm for ^{1}H-NMR and 77.0 ppm for ^{13}C-NMR) or DMSO 2.50 ppm for ^{1}H-NMR and 39.5 ppm for ^{13}C-NMR). The coupling constants (*J*) are reported in Hertz (Hz). IR spectra were recorded by using a Perkin-Elmer Spectrum 100 FT-IR spectrometer with diamond ATR accessory as thin film. Mass spectra were recorded using electrospray ionization (ESI).

2. Preparation azidoiodobenzenes

2.1. 4-azidoiodobenzene (7)

A round bottom flask was charged with 4-iodoaniline (**5**, 3 g, 13.7 mmol, 1.0 eqv.) and water (15.2 mL, 0.90 M). Concentrated HCl (2.5 mL 2.1 eqv.) was added to vigorously stirred reaction mixture in an ice-water bath. A pre-cooled solution of $NaNO_2$ (0.95 g, 13.7 mmol, 1.0 eqv.) in water (5.50 mL, 2.50 M) was added dropwise to the reaction mixture, after which time the reaction mixture was stirred for 15 min. The solution of NaN_3 (0.89 g, 13.7 mmol, 1.0 eqv.) in water (5.50 mL 2.50 M) was added dropwise to the reaction mixture while maintaining the temperature in the ice bath, and then the reaction mixture was stirred an additional 20 min at 0 °C, then stirred at rt for another 3 h. The reaction mixture was extracted with EtOAc (2x50 mL) and the aqueous layer was adjusted to pH 8-10 with $NaHCO_3$ before discarding. The combined organic solution was washed with water and brine and dried over Na_2SO_4, filtered and concentrated under reduced pressure. The crude azidoiodobenze derivative was further purified by flash column chromatography over silica gel with 0-5% ethylacetate/hexanes as eluent to afford 4-azidoiodobenze (**7**, 2.60g, 78%). ^{1}H NMR (400 MHz, $CDCl_3$) δ 7.63 (d, *J* = 8.7 Hz, 2H), 6.77 (d, *J* = 8.7 Hz, 2H). ^{13}C NMR (101 MHz, $CDCl_3$) δ 140.06, 138.79, 121.14, 88.31.

2.2. 3-azidoiodobenzene (6)

3-azidoiodobenzene (**6**, 2.80 g, 69%) was prepared from 3-iodoaniline in a manner analogous to that described for 4-azidoiodobenzene. ^{1}H NMR (400 MHz, $CDCl_3$) δ 7.46 (ddd, *J* = 7.8, 1.6, 0.9 Hz, 1H), 7.41 – 7.32 (m, 1H), 7.06 (td, *J* = 7.9, 0.8 Hz, 1H), 6.98 (ddt, *J* = 8.1, 2.0, 0.9 Hz, 1H). ^{13}C NMR (100 MHz, $CDCl_3$) δ 141.33, 133.91, 131.04, 127.89, 118.39, 94.61.

3. Preparation of substituted furfuraldehydes

3.1. 5-(4-azidophenyl)furan-2-carbaldehyde (10)

To a vial containing 4-azidoiodobenzene (**7**, 0.50 g, 2.04 mmol, 1 eqv.), furfural-boronic acid **8** (0.37 g, 2.65 mmol, 1.30 eqv.), and bis(triphenylphosphine)palladium(II) dichloride (0.10 g, 0.10 mmol, 5 mol%) was added EtOH (1.00 mL), DME (0.61 mL), and 2M aqueous Na_2CO_3 (1.8 mL). The reaction mixture was heated in an oil bath at 65 °C for 1 h. The mixture was diluted with H_2O and extracted three times with ethyl acetate. The combined organic layers were washed with brine, dried over Na_2SO_4, filtered and concentrated. The crude product was purified by column chromatography (5-15% ethyl acetate/hexanes) to afford 5-(4-azidophenyl)furan-2-carbaldehyde (**10**, 0.25 g, 1.17 mmol, 56%): ^{1}H NMR (400 MHz, $CDCl_3$) δ 9.64 (s, 1H), 7.82 (d, *J* = 8.6 Hz, 2H), 7.33 (d, *J* = 3.8 Hz, 1H), 7.16 – 7.02 (m, 2H), 6.81 (d, *J* = 3.7 Hz, 1H). ^{13}C NMR (100 MHz, $CDCl_3$) δ 177.20, 158.72, 152.03, 141.46, 126.95, 125.81, 119.68, 107.59.

3.2. 5-(3-azidophenyl)furan-2-carbaldehyde (9)

5-(3-azidophenyl)furan-2-carbaldehyde (**9**, 0.25 g, 57%) was prepared from 3-azidoiodobenzene (**6**) in a manner analogous to that described for 5-(4-azidophenyl)furan-2-carbaldehyde (**10**). ^{1}H NMR (400 MHz, $CDCl_3$) δ 9.67 (s, 1H), 7.58 (ddd, *J* = 7.8, 1.6, 0.9 Hz, 1H), 7.47 – 7.39 (m, 2H), 7.33 (d, *J* = 3.8 Hz, 1H), 7.06 (ddd, *J* = 8.1, 2.2, 1.0 Hz, 1H), 6.87 (d, *J* = 3.7 Hz, 1H). ^{13}C NMR (101 MHz, $CDCl_3$) δ 177.34, 158.04, 152.21, 140.98, 130.57, 130.35, 121.72, 119.95, 115.59, 108.46.

4. Preaparation of pyrazolone 3

4.1. 2-chloro-5-hydrazinobenzoic acid hydrochloride

To a solution of 5-amino-2-chlorobenzoic acid (**1**, 2.50 g, 14.6 mmol) in concentrated HCl (10 mL) at 0 °C was slowly added a solution of $NaNO_2$ (1.21 g, 17.5 mmol) in water (5.0 mL) at a rate that maintained the solution temperature below 5-10 °C. After stirring for 30 min, a

solution of tin chloride dihydrate (8.20 g, 36.4 mmol) in water (5.0 mL) and concentrated HCl (10 mL) was added a rate that maintained below 5-10 °C. The viscous mixture was diluted with an additional 10 mL of concentrated HCl and 5.0 mL of water and stirred an additional 4 h at 5-10 °C. The crude mixture was then filtered, and collected solids were recrystallized from hot water (60 mL) to provide 2-chloro-5-hydrazinobenzoic acid hydrochloride (**2**, 1.5 g, 55%) ^{1}H NMR (400 MHz, DMSO-d_6) δ 10.50 (s, 3H), 8.68 (s, 1H), 7.58 – 7.25 (m, 2H), 7.13 (dd, J = 8.7, 2.8 Hz, 1H), 3.45 (s, 2H). ^{13}C NMR (100 MHz, DMSO-d_6) δ 167.10, 145.11, 132.16, 131.60, 123.79, 118.80, 116.52.

4.2. 2-chloro-5-(5-oxo-3-(trifluoromethyl)-2,5-dihydro-1*H*-pyrazol-1-yl)benzoic acid (3)

To a solution of 2-chloro-5-hydrazinobenzoic acid hydrochloride (**2**, 0.75 g, 3.36 mmol, 1 eqv.) and ethyl 4,4,4-trifluoroacetoacetate (0.49 mL, 3.36 mmol, 1 eqv.) in acetic acid (3.4 mL, 1.0 M) was added triethylamine (0.49 mL, 3.36 mmol, 1 eqv.). The resulting mixture was heated at reflux for 24 h. The excess acetic acid was evaporated under reduced pressure, resulting in viscous oil. The crude product triturated by addition of DCM, filtered, and dried under vacuum to afford pyrazolone **3** (0.74 g, 72%). ^{1}H NMR (400 MHz, DMSO-d_6) δ 13.34 (s, 1H), 8.18 (d, J = 2.7 Hz, 1H), 7.94 (dd, J = 8.8, 2.8 Hz, 1H), 7.70 (d, J = 8.7 Hz, 1H), 5.98 (s, 1H), 3.39 (s, 1H).

5. Preparation EN460 derivatives PB-10 and PB-11

5.1. (*E*)-5-(4-((5-(4-azidophenyl)furan-2-yl)methylene)-5-oxo-3-(trifluoromethyl)-4,5-dihydro-1*H*-pyrazol-1-yl)-2-chlorobenzoic acid (PB-11)

To a solution of 2-chloro-5-(5-oxo-3-(trifluoromethyl)-2,5-dihydro-1*H*-pyrazol-1-yl)benzoic acid (**3**, 104.3 mg, 0.49 mmol, 1 eqv.) and 5-(4-azidophenyl)furan-2-carbaldehyde (**10**, 150.0 mg, 0.49 mmol, 1 eqv.) in acetic acid (0.98 mL, 0.5 M) was added catalytic amount of

NaOAc (4.0 mg, 49 μmol, 0.1 eqv.). The resulting mixture was heated to reflux for 3 h. The excess acetic acid was evaporated under reduced pressure, followed by trituration by addition of a water-methanol mixture. The crude product was filtered and washed with water to afford **PB-11** as a reddish solid (127.9 mg, 52%) ^{1}H NMR (400 MHz, DMSO-d_6) δ 12.15 (s, 1H), 8.70 (s, 1H), 8.30 (dd, *J* = 11.1, 2.7 Hz, 1H), 8.10 – 7.94 (m, 1H), 7.92 – 7.46 (m, 6H), 7.22 (dd, *J* = 8.0, 2.4 Hz, 1H).

5.2. (*E*)-5-(4-((5-(3-azidophenyl)furan-2-yl)methylene)-5-oxo-3-(trifluoromethyl)-4,5-dihydro-1*H*-pyrazol-1-yl)-2-chlorobenzoic acid (PB-10)

PB-10 (231.0 mg, 93%) was prepared from 2-chloro-5-(5-oxo-3-(trifluoromethyl)-2,5-dihydro-1*H*-pyrazol-1-yl)benzoic acid (**3**) and 5-(3-azidophenyl)furan-2-carbaldehyde (**9**) in a manner analogous to that described for **PB-11**. ^{1}H NMR (400 MHz, DMSO-d_6) δ 13.66 (s, 1H), 8.30 (dd, *J* = 11.9, 2.7 Hz, 1H), 8.13 – 7.95 (m, 2H), 7.91 – 7.83 (m, 1H), 7.78 (s, 1H), 7.69 – 7.58 (m, 2H), 7.37 – 7.18 (m, 2H).

MTT Assay

Cells were seeded at 15,000 cells per well in 96-well plate and cells are incubated with DMSO or increasing concentrations of EN460, PB-10, and PB-11 (0.78, 1.56, 3.13, 6.25, 12.5 and 50 μM) for 72h. Afterwards, 50 μl of MTT (2 mg/ml) was added to each well and incubated for 4h. The formazan crystals in viable cells were dissolved by using dimethyl sulfoxide (DMSO, 50 μl per well). The absorbance of each well was measured using a microplate reader (Spectramax 190, USA) at 570 nm. All the experiments were performed in triplicate.

Western blot analysis

U266 cells were incubated with DMSO or EN460 for 2, 4 and 8h and cell lysates were collected (n=3 independent assays). Protein extracts was separated in 8-10% SDS-PAGE gel and

transferred onto a PVDF membrane (Millipore, MA) and incubated with 5% nonfat milk in tris-buffered saline with Tween 20 (TBST) buffer for 1 h at room temperature. Membranes were then incubated for overnight at 4°C with different antibodies: p-EIF2alpha (3597), ATF4 (11815) and ATF6 (65880) were purchased from Cell Signaling Technology (Boston, MA) and beta-actin (A2228) was purchased from Sigma-Aldrich. Blots were then incubated with secondary anti-mouse or anti-rabbit HRP labeled antibodies (Jackson ImmunoResearch Laboratories, Westgrove, PA, USA) for 1h. The membrane was developed and protein signals were detected using chemiluminescence (Amersham Imager 600, GE).

Annexin V/propidium iodide (PI) double-staining assay

Apoptosis was measured by flow cytometry using Annexin V/PI double staining to detect apoptotic cells. U266 cells were treated with DMSO or EN460 for 18h. Cells were harvested and washed with ice-cold PBS and resuspended in 1X binding buffer containing Annexin V and PI for 15 min at 37°C in the dark. Stained cells were quantified by flow cytometry. At least 10,000 cells were analyzed for each sample (n=3 independent assays).

MM Patient Cohort

Series GSE9782 was downloaded from the Gene Expression Omnibus (GEO). Gene expression data consists of Affymetrix HG-U133A and HG-U133B GeneChip arrays. Normalized, processed data was used from GEO; array processing is described in Mulligan, et al. There were 264 patients profiled, including 76 Dexamethasone-treated and 188 bortezomib-treated patients. Two probesets are reported to detect Ero1L (218498_s_at and 222646_s_at). We use 222646_s_at as it had the largest average expression (306.99101). Differences in outcomes (overall survival) were determined by stratifying the patient population on median Ero1L

expression (222646_s_at). A Kaplan-Meier survival curve was generated based on these groupings, and a log-rank test was performed to assess statistical significance.

Results and Discussion

In this study, we evaluated the role of Ero1L as potential drug target in MM. Additionally, we further evaluated the Ero1L inhibitor EN460 as proof of principle for movement into novel chemotherapeutic space, and developed two additional EN460 derivatives (PB-10 and PB-11) as a tool set to probe biological activity. To determine whether Ero1L expression was a poor prognostic indicator for the treatment of MM we utilized a publically available data set that was generated from several Phase II-III trials (024, 025, 039, 040) which either assessed Bortezomib or compared Bortezomib to high dose dexamethasone treatment[17]. Briefly, patients were consented for genomic analyses of pretreatment tumor samples. In GSE9782, all patients receiving bortezomib (n=188) were compared for differences in outcome related to *ERO1L* expression levels. Kaplan-Meier estimates were calculated for overall survival in the high (>median *ERO1L* expression) and low (<median *ERO1L* expression) groups. A log-rank test was used to assess significant difference in outcome, and a Cox regression of the dichotomous variable (high *vs.* low) was used to estimate a hazard ratio and confidence interval. Patients had one or more prior therapies. Correlations of high *ERO1L* alpha expression and poor outcome extended to both bortezomib and dexamethasone treated patients (See **Figure 1 p<0.01**). Thus, *ERO1L* alpha may be a marker of drug resistance or tumor progression independent of the mechanism of action of the drug. Collectively, these data suggest that *ERO1L* alpha is predictive in the setting of relapsed MM patients and maybe a good marker for stratifying patients to receive novel therapies versus additional standard of care agents.

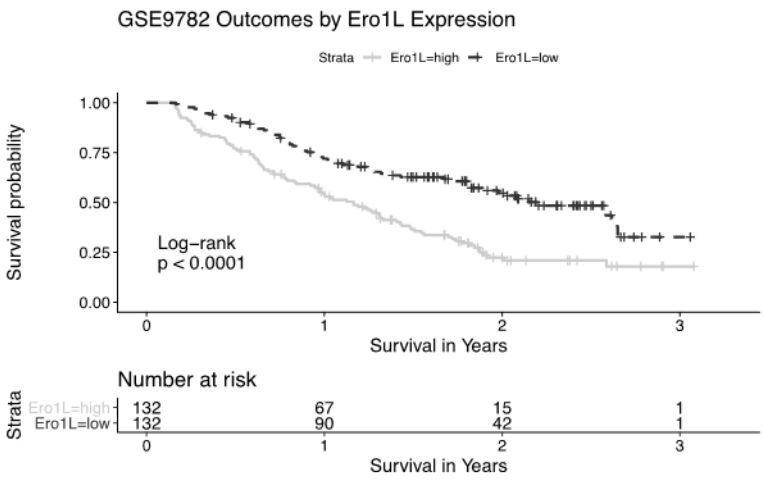

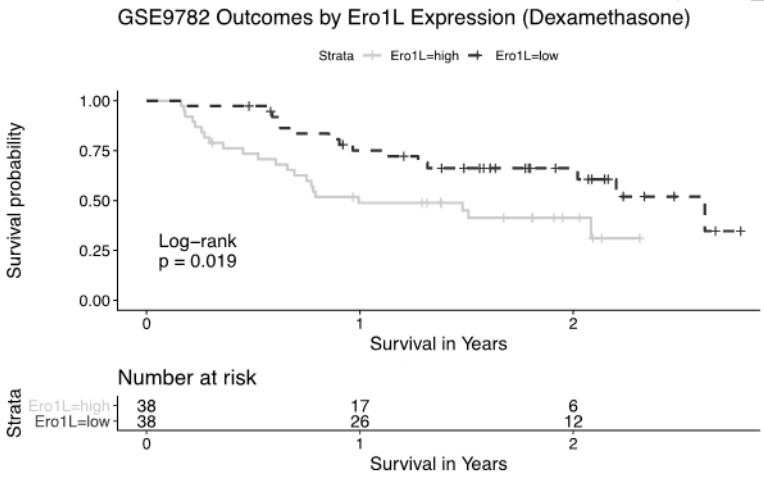

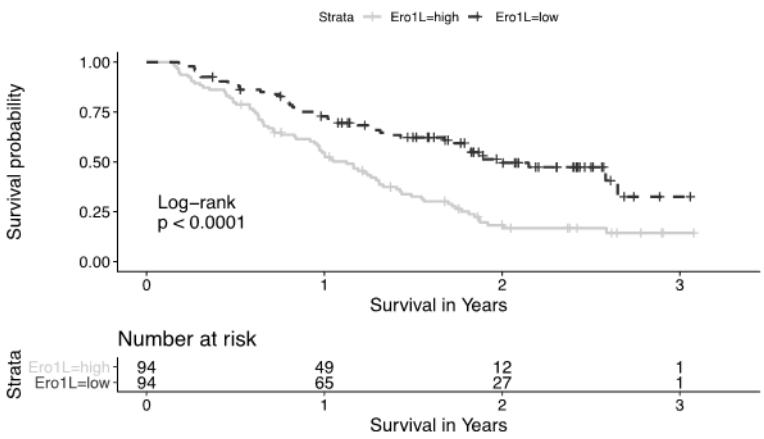

Figure 1: High Ero1L expression levels are poor prognostic indicator of survival in relapsed MM patients. (A) GSE9782, all patients were compared for differences in outcome related to ERO1L expression levels. Kaplan-Meier estimates were calculated for overall survival in the high (>median ERO1L expression) and low (<median ERO1L expression) groups. A log-rank test was used to assess significant difference in outcome. **(B)** Patients receiving Dexamethasone (n=76). **(C)** Patients receiving bortezomib (n=188).

Biological characterization of the Ero1L inhibitor[12] EN460 was performed in U266 MM cancer cells. As shown in Figure 2, EN460 induces apoptosis in the MM U266 cells as detected by the percentage of Annexin V positive cells. This finding correlates with the induction of ER stress as measured by induction of p-EIF2 alpha and reduction of full length ATF6. However, considering the lack of specificity of EN460, novel probes are required to further validate whether targeting Ero1L as a single target is sufficient to induce ER stress and cell death in MM cells. Furthermore, we found that treatment with EN-460 of normal PBMCs was sufficient to induce cell death (data not shown). Due to the lack of specificity of EN-460, it is difficult to assess whether the toxicity is due to on target or off-target effects and thus supports the need to develop more specific ERO1L compounds, which do not inhibit other FAD containing enzymes to enable pharmacological validation of the target for the treatment of cancer.

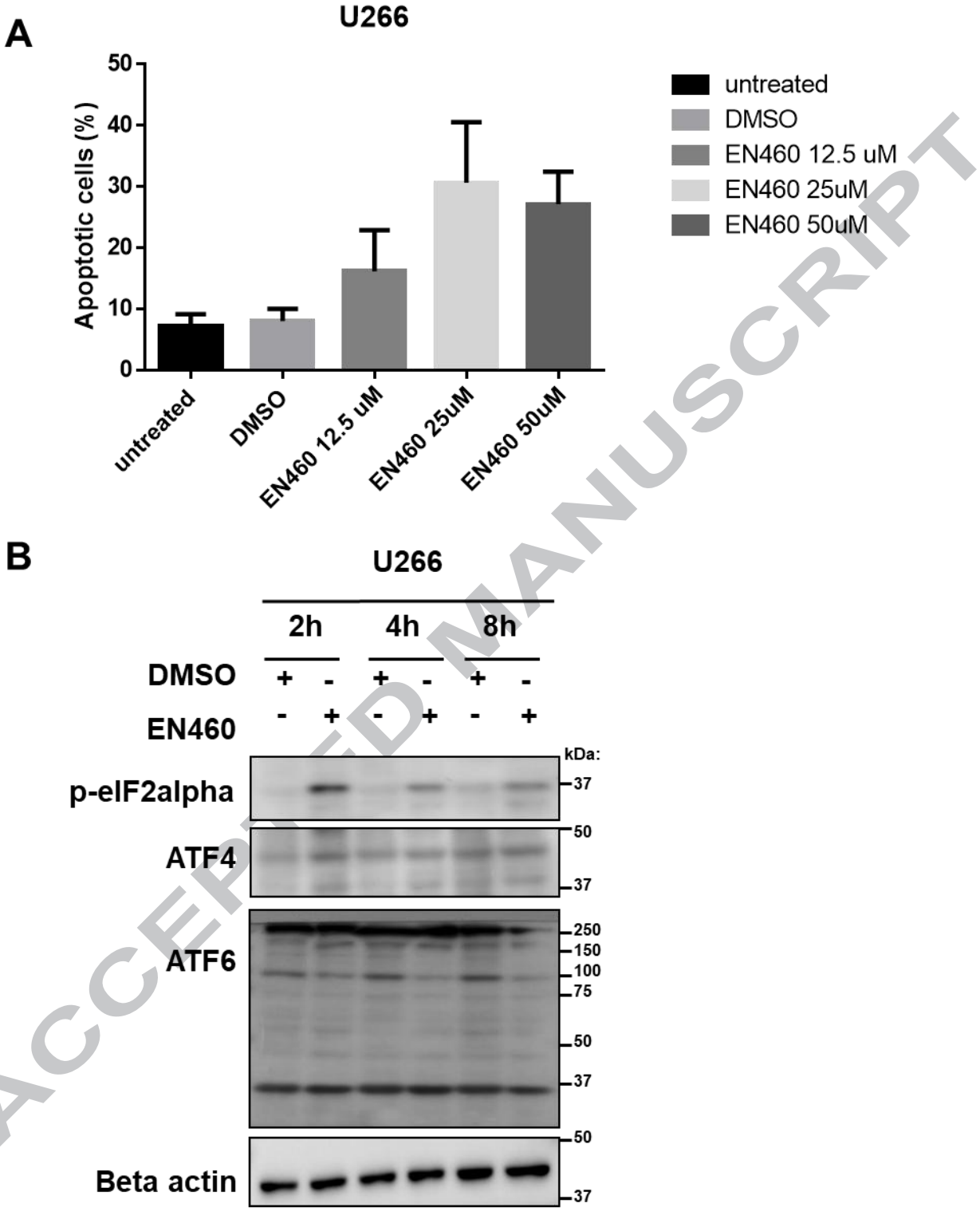

Figure 2: ERO1L inhibitor, EN460, induces apoptosis and ER stress in MM cells. (A) U266 cells were treated with DMSO (vehicle control) or 25 μM EN460 for 18 h and then subjected to Annexin V-FITC and propidium iodide (PI) staining followed by flow cytometry analysis of apoptosis. Data are reported as means ± SD for three independent experiments. **(B)** U266 cells were treated with DMSO (vehicle control) and EN460 for 2, 4 and 8 h. Markers for the induction of ER stress include an increase in phosphorylation of eIf2 alpha, increased ATF4 levels and cleavage of ATF6. As such we measured the induction of these ER stress proteins following treatment of EN-460. Following exposure to EN-460 we observed a robust increase in p-eIF2α and a reduction of full length AYF6. The ATF6 antibody used does not recognize the cleaved product but as shown EN-460 treatment of U266 cells resulted in reduced levels of full length ATF6 consistent with cleavage of the protein. Surprisingly only a modest increase in ATF4 was detected following treatment with EN-460 in U266 cells. Equal protein loading is demonstrated by beta actin (n=3 independent experiments).

Considering the clinical data showing that high Ero1L expression levels are a poor prognostic indicator of survival, the development of chemical probes targeting Ero1L are warranted to validate whether targeting Ero1L is a tractable strategy for the treatment of multiple myeloma. To date few studies have focused on the identification and development of novel Ero1L inhibitors. The first paper published on this topic identified the inhibitor EN460, which inhibited the enzyme in the low micromolar range.[11] Ero1L and PDI work in concert to form the protein folding via disulfide bonds.[13, 18] Figure 3 shows the docked Ero1-PDI protein-protein interaction site as determined via docking using the Gramm-X protein docking server, showing the interaction between the transfer faces of the two proteins.[19] Since the crystal structure of

Ero1L (hyperactive 3AHQ) does not have the full sequence we modeled the extra loops with YASARA (www.yasara.com).

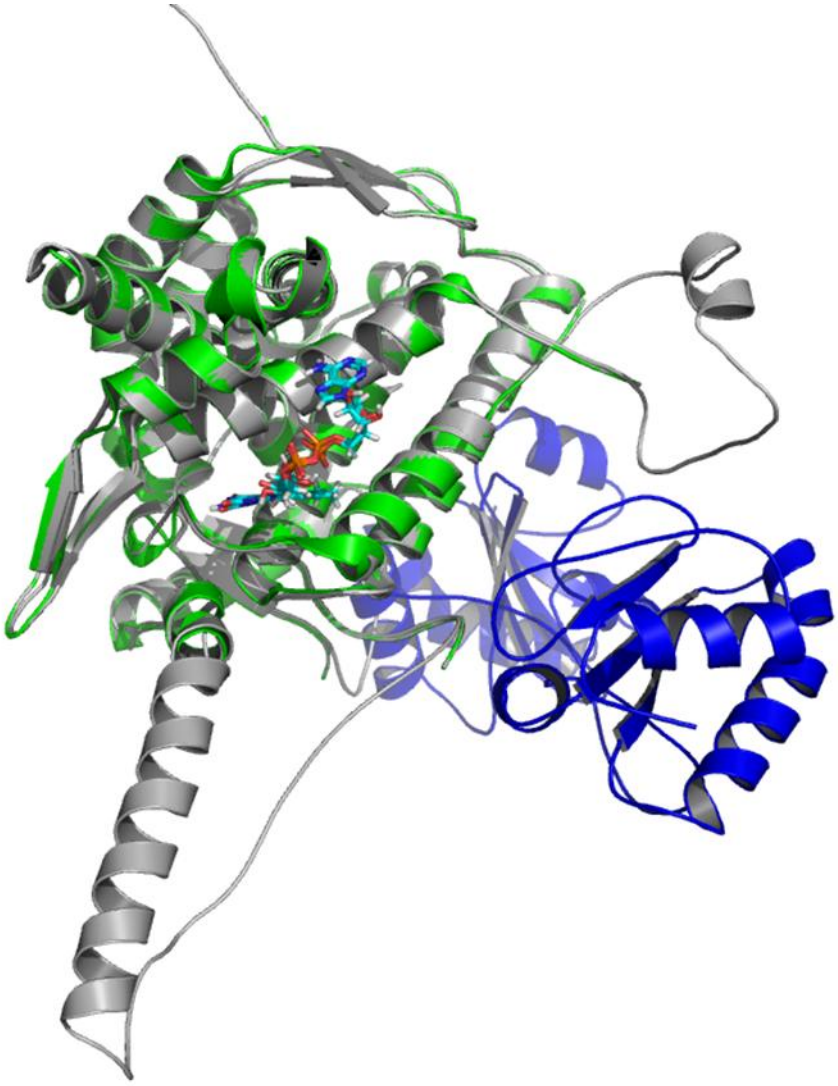

Figure 3: Protein-protein interaction (PPI) of Ero1L and PDI. The docked pose showing the orientation of the two proteins docked to allow for the redox cycling and electron transfer. Ero1L with the full sequence modeled onto 3AHQ, is shown as silver, and PDI as blue. The

crystal structure of Ero1L the missing sequence is shown in green. The FAD ligand is shown in atomic colors.

The EN460 compound has poor solubility, which does not allow for reaching >200 uM concentrations *in vitro*. To gain insight into the structural features important for interaction with Ero1L we screened two derivatives: AK968 and AN968. AN968 was found to be marginally active (See Supplementary Fig. 2), while the derivative AK968 was inactive. We concluded that the 3-carboxyalic acid group closest to the pyrazole was an important feature since AN968 was less active than EN460, and removal of the carboxylic acid group from AK968 resulted in complete loss of compound activity. We designed and prepared two azide derivatives of EN460: PB-10 and PB-11. These probe molecules compounds were designed to increase versatility through the inclusion of functionalizable handles (Scheme 1). Our hypothesis was that these EN460 derivatives would have similar activity as compared to EN460. Compound PB-10, the *meta*-azido isomer, was comparable in solubility to EN460. On the other hand, the *para*-azido isomer PB-11 was less soluble in physiological buffers (e.g. PBS pH 7.4) and therefore was not used for subsequent bioassay experiments.

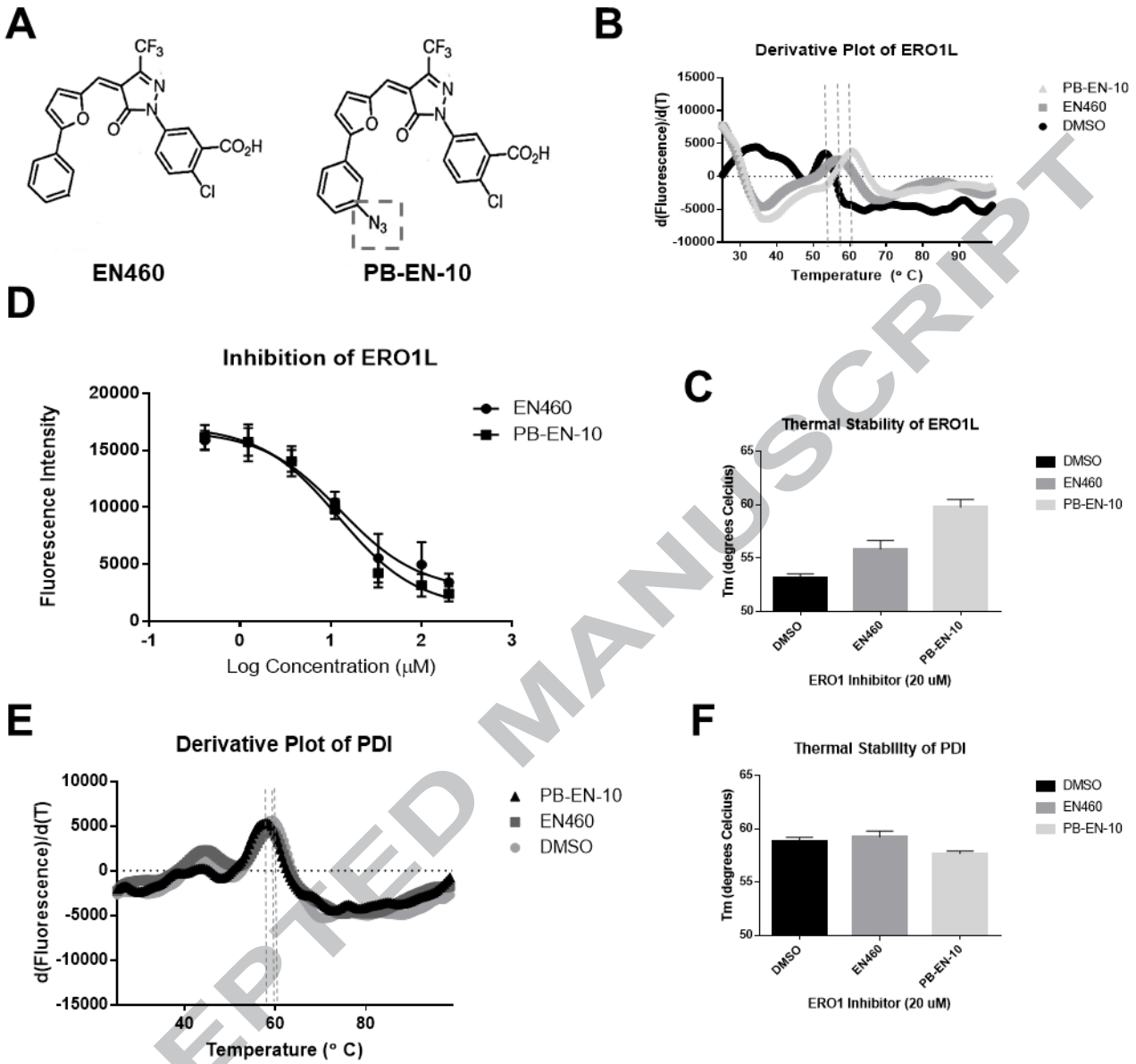

Figure 4 . Azide modification of EN460 increased efficacy. **(A)** Structural formulas of EN460 and PB-EN-10 (an azide derivative of EN460). **(B)** PB-EN-10 shifts first derivatives, dF/dT of melt curve compared to vehicle (DMSO). Graph of first derivatives, dF/dT, of fluorescence intensities of Sypro Orange combined with Ero1α (0.25 mg/mL) and PB-EN-10 (20 μM) or DMSO. Melting temperatures (Tm) were defined by inflection point in dF/dT (dashed lines). **(C)**

Bar graph of melting temperatures (Tm) of Ero1α with PB-En-10 (20 μM), EN460 (20 μM), or DMSO. Ero1α/PB-EN-10 interaction increased Tm and stability of Ero1α compared to EN460. **(D)** PB-EN-10 improved inhibition of hEro1α activity compared to parent compound, EN460. Purified human Ero1α (0.0625 mg/mL) incubated with increasing concentrations of EN460 or PB-EN-10 with Amplex Red Assay. **(E**) Graph of first derivatives, dF/dT of melt curves and **(F)** Melting temperatures (Tm) of PDI (0.25 mg.mL) were not altered with the addition of 20 μM of PB-EN-10 or EN460 suggesting the inhibition of Ero1α was not mediated by PDI. Graphs are represented images of two experiments performed in triplicate.

We characterized the inhibition of Ero1L by EN460 and the azide derivative PB-10 (Figure 4A) by enzymatic and thermal shift assays. Both EN-460 and PB-10 inhibited Ero1L enzymatic activity in a similar dose dependent manner (see Figure 4B). The interaction between Ero1L and EN460 was further evaluated by thermal shift assay (Figure 4C-D). The protein and ligand is co-incubated and heated where the increased loss of 3D structure (denaturation) allows for the fluorescent probe SYPRO Orange to bind and fluorescence. A shift in melting temperature shows stabilization of the protein and therefore binding to the protein. The Tm for Ero1L with addition of DMSO (2% DMSO vehicle control 53.15 °C +/- 0.15 SEM) EN460 (55.86 °C +/- 0.3 SEM) and PB-10 (59.76 °C +/-0.27 SEM) was able to shift the melting temperature indicating a stabilization effect on the Ero1L structure (Figure 4C-D). The Tm of PDI was not significantly altered with the addition of EN460 (59.21 °C +/- 0.24 SEM) or PB-10 (57.67 °C +/- 0.11 SEM) compared to control (DMSO, 58.86 °C +/- 0.12 SEM) suggesting EN460 and PB-10 do not bind and stabilize PDI (Figure 4E and 4F). Together these data indicate that neither EN-460 nor PB-

10 shifted the PD1 melt curve, and enzymatic inhibition was due to binding Ero1Lα and not PDI (Figure 4E-F).

Interestingly, the increase in stability due to PDI/PB-10 interaction did not affect the activity of Ero1L *in vitro*. The IC50 determined by enzymatic Amplex Red assay were similar between PB-10 (IC_{50} = 12.19 µM) and EN460 (IC_{50} = 12.74 µM). U266 and MM1.S cells exposed to EN460 had IC_{50}'s, of 10.1 µM +/-1.11 and 14.74 µM +/- 1.23 respectively, compared to PB-10 (14.73 µM 14.73 +/- 1.1 and 18.76 µM +/- 1.06) (Table 1).

Table 1: Determination of IC50 value of EN460 and its derivatives, PB-EN-10, PB-EN-11, in U266 and MM1.s cells. The cell viability was determined by MTT assay after treatment with EN460 and its derivatives for 72 h and then IC50 was calculated. Results are mean ± SD values for 3 independent experiments.

	IC50 (uM),		
MM cell lines	EN460	PB-EN-10	PB-EN-11
U266	10.1±1.11	14.73±1.1	7.03±1.14
MM1.S	14.74±1.23	18.76±1.06	17.26±1.1

To date the full spectrum of EN460 activity for FAD containing enzymes have not been studied. Since Ero1L is an FAD containing enzyme, several other FAD containing enzymes have been characterized as drug targets for the treatment of a variety of diseases. To delineate the selectivity of EN460, we tested it against four classical FAD containing enzymes, including monoamine oxidase A and B (MAO-A and MAO-B), as well as Lysine-specific histone

demethylase 1A (LSD1; lysine (K)-specific demethylase 1A (KDM1A)). Figure 5 shows that EN460 inhibited the FAD containing enzymes in the low microM range, IC_{50}: Ero1 = 22.13 uM, MAO-A = 7.9 uM, MAO-B = 30.59 uM, and LSD-1 = 4.16 uM. Both MAO-A and LSD1 have high sequence similarity so it was not surprising to see inhibition at the same level for the two enzymes.

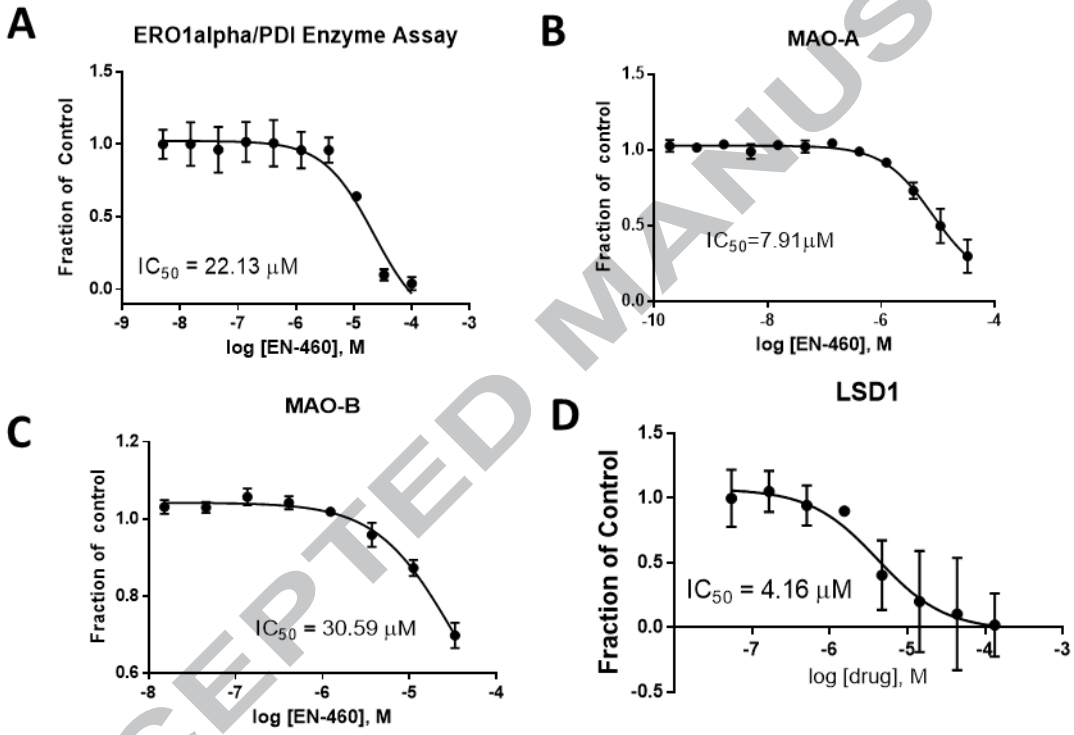

Figure 5: Inhibition of FAD containing enzymes activity with EN460.(A) Ero1L **(B)** MAO-A **(C)** MAO-B **(D)** LSD-1. Each data point is avg. and standard error of fit, with N = 2.

Figure 6 shows the enzyme-inhibition kinetics, with EN-460 inhibiting Ero1L in a competitive manner based on the analysis of the increased substrate PDI with different combination of EN460 concentrations, resulting in a Km, which was increased, but the Vmax largely stated the same.

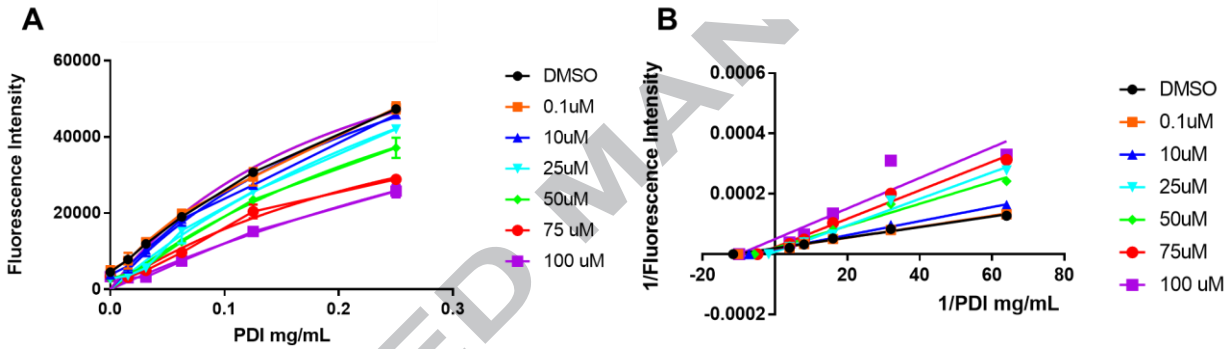

Figure 6. Enzyme kinetics of EN460 inhibition of Ero1α oxidase. Ero1α activity was monitored by using an Amplex Red assay. **(A)** The elevated hydrogen peroxide levels (intensifying fluorescence) observed with increasing concentrations of purified human PDI protein were progressively suppressed in the presence of escalating amounts of EN460. **(B)** Lineweaver–Burk plot of results in (A) shows EN460 functions as a competitive inhibitor of Ero1α, under these conditions.

To gain insight into the different binding modes, molecular docking studies were performed. EN460 bound to the FAD pocket of Ero1L through hydrogen bonding to TRP197 and ARG287, and hydrophobic interactions between the aromatic groups and CYS397 and ARG287 (Figure 7).

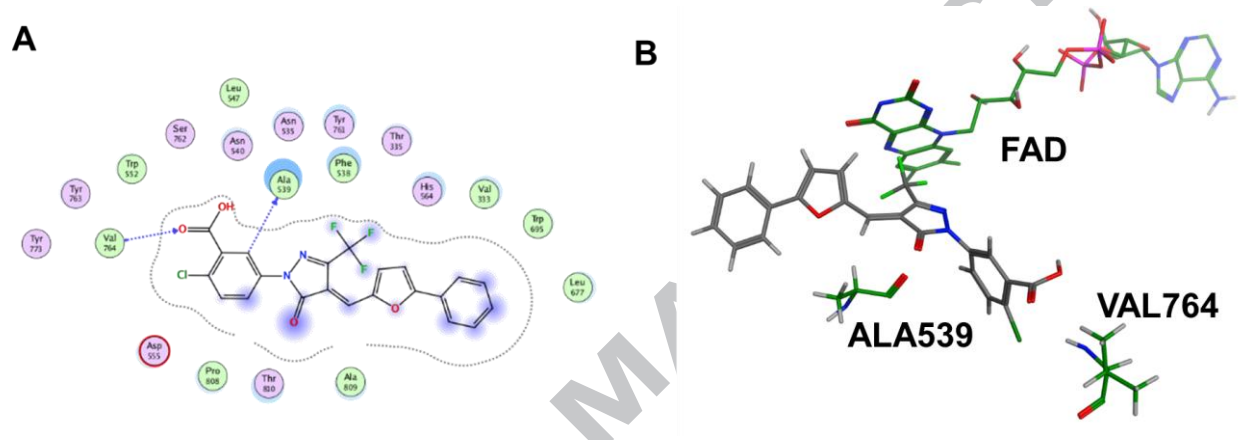

Figure 7: Docking of EN460 in FAD binding pocket of Ero1L. (A) Hyperactive form of Ero1α (DOI: 10.2210/pdb3AHQ/pdb) was used to determine possible binding of EN460 in FAD binding pocket with PyMol (Schrödinger). **(B)**

In the enzyme MAO-A, a hydrogen bond with SER209 was predicted, while the aromatic ring of EN460 was sandwiched between the aromatic rings of TRY407 and TRY444 (Figure 8). MAO-B binding was achieved through aromatic interactions with no hydrogen bonding predicted, which would account for the lower inhibition (~30 uM) (Figure 8).

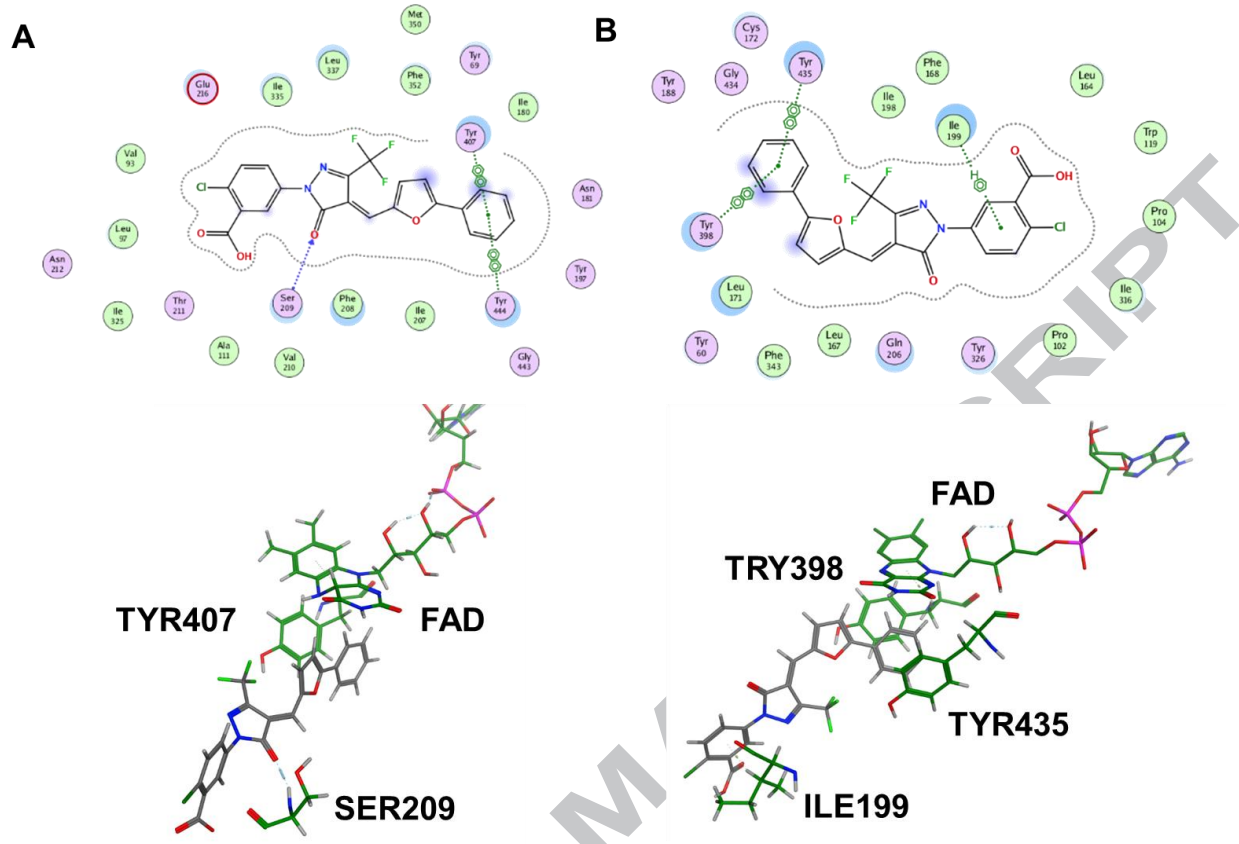

Figure 8 Docking of EN460 in binding pockets of other FAD containing enzymes (A) Monoamine oxidase A (MAO-A) **(B)** Monoamine oxidase B (MAO-B).

Lastly, the FAD containing enzyme LSD1 was also docked with EN460, and found it docked through hydrogen bonding with VAL764 and an aromatic interaction with ALA539 (Figure 9). Considering the close homology between MAO-A and LSD1 it not surprising that they share similar IC_{50} values, with LSD1 only slightly more inhibited by EN460. LSD1 is also known as KDM1A and is a FAD demethylase, where it removes methyl groups from histone 3 protein

H3K4me2/1 and H3K9me2/1. LSD1 has recently gained more attention as a possible cancer drug target.[20]

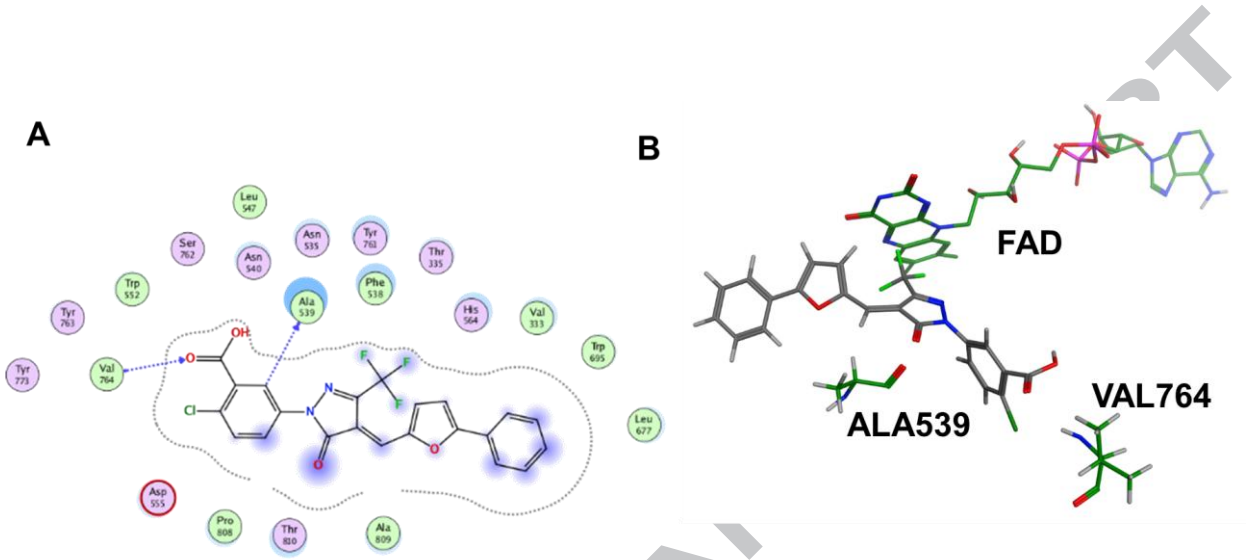

Figure 9: Docking of EN460 in FAD binding pocket of LSD1. (A) ligand interaction diagram showing interactions with Val764 and Ala539; (B) docked pose of EN460 in LSD1**.**

Taken together, considering the lack of specificity of EN-460, novel probes are required to fully validate whether targeting Ero1L as a single target is sufficient to induce ER stress and cell death in MM cells while sparing normal cells.

Conclusion

In this study, we show that the FAD containing ER protein Ero1L expression is a prognostic indicator for MM patients relapsing on therapy, with increased Ero1L expression associated with shorter survival times. We propose that Ero1L is a putative novel drug target in MM cancers. Others have identified PDI as a potential target for the treatment of MM.[21] One potential

advantage of targeting Ero1L over PDI is that PDI consists of multiple family members and thus redundancy maybe problematic with respect to emergence of drug resistance. We anticipate that the lead compounds EN460 and PB-10 can be used to develop more potent and specific inhibitors of Ero1L. Moreover, the azide functional group handle of PB-10 allows it to be used as a tool for potential development of further analogues and exploration of SAR using Click chemistry to increase the complexity of the molecule for design of increased affinity toward ERO1L compared to other FAD containing enzymes. Future studies will be aimed at developing selective EN460 analogs that do not cross-react with the monoamine oxidase family of enzymes, which will allow for more robust evaluation of the target in cancers.

Acknowledgements

The work was supported by the NIH, as a NCI grant (LH RO1 CA195727). The grant number is the WVU Stroke CoBRE grant P20 GM109098 (WG). Also, supported by the NIH Grant P20 GM103434 to the West Virginia IDeA Network for Biomedical Research Excellence. The project described was supported by the National Institute of General Medical Sciences, U54GM104942. This work has been supported in part by the Chemical Biology Core/Structural Biology Unit at the H. Lee Moffitt Cancer Center & Research Institute, an NCI designated Comprehensive Cancer Center (P30-CA076292). GBD acknowledged The Estate of Dr. William Price Bittinger for support of the Experimental therapeutics synthesis collaborative.

References

[1] K.C. Anderson, R.A. Kyle, W.S. Dalton, T. Landowski, K. Shain, R. Jove, L. Hazlehurst, J. Berenson, Multiple Myeloma: New Insights and Therapeutic Approaches, Hematology (Am Soc Hematol Educ Program), (2000) 147-165.
[2] T. Hideshima, P. Richardson, D. Chauhan, V.J. Palombella, P.J. Elliott, J. Adams, K.C. Anderson, The proteasome inhibitor PS-341 inhibits growth, induces apoptosis, and overcomes drug resistance in human multiple myeloma cells, Cancer research, 61 (2001) 3071-3076.
[3] D.J. Kuhn, Q. Chen, P.M. Voorhees, J.S. Strader, K.D. Shenk, C.M. Sun, S.D. Demo, M.K. Bennett, F.W. van Leeuwen, A.A. Chanan-Khan, R.Z. Orlowski, Potent activity of carfilzomib, a novel, irreversible inhibitor of the ubiquitin-proteasome pathway, against preclinical models of multiple myeloma, Blood, 110 (2007) 3281-3290.
[4] S. Gandolfi, J.P. Laubach, T. Hideshima, D. Chauhan, K.C. Anderson, P.G. Richardson, The proteasome and proteasome inhibitors in multiple myeloma, Cancer Metastasis Rev, 36 (2017) 561-584.
[5] C.T. Wallington-Beddoe, M. Sobieraj-Teague, B.J. Kuss, S.M. Pitson, Resistance to proteasome inhibitors and other targeted therapies in myeloma, Br J Haematol, 182 (2018) 11-28.
[6] S.V. Rajkumar, S. Kumar, Multiple Myeloma: Diagnosis and Treatment, Mayo Clin Proc, 91 (2016) 101-119.
[7] R. Noiva, Protein disulfide isomerase: the multifunctional redox chaperone of the endoplasmic reticulum, Semin Cell Dev Biol, 10 (1999) 481-493.
[8] R.M. Robinson, L. Reyes, R.M. Duncan, H. Bian, A.B. Reitz, Y. Manevich, J.J. McClure, M.M. Champion, C.J. Chou, M.E. Sharik, M. Chesi, P.L. Bergsagel, N.G. Dolloff, Inhibitors of the protein disulfide isomerase family for the treatment of multiple myeloma, Leukemia, (2018).
[9] P.E. Lovat, M. Corazzari, J.L. Armstrong, S. Martin, V. Pagliarini, D. Hill, A.M. Brown, M. Piacentini, M.A. Birch-Machin, C.P. Redfern, Increasing melanoma cell death using inhibitors of protein disulfide isomerases to abrogate survival responses to endoplasmic reticulum stress, Cancer Res, 68 (2008) 5363-5369.
[10] A.M. Benham, M. van Lith, R. Sitia, I. Braakman, Ero1-PDI interactions, the response to redox flux and the implications for disulfide bond formation in the mammalian endoplasmic reticulum, Philos Trans R Soc Lond B Biol Sci, 368 (2013) 20110403.
[11] B.P. Tu, J.S. Weissman, The FAD- and O(2)-dependent reaction cycle of Ero1-mediated oxidative protein folding in the endoplasmic reticulum, Mol Cell, 10 (2002) 983-994.
[12] J.D. Blais, K.T. Chin, E. Zito, Y. Zhang, N. Heldman, H.P. Harding, D. Fass, C. Thorpe, D. Ron, A small molecule inhibitor of endoplasmic reticulum oxidation 1 (ERO1) with selectively reversible thiol reactivity, J Biol Chem, 285 (2010) 20993-21003.
[13] K. Inaba, S. Masui, H. Iida, S. Vavassori, R. Sitia, M. Suzuki, Crystal structures of human Ero1alpha reveal the mechanisms of regulated and targeted oxidation of PDI, EMBO J, 29 (2010) 3330-3343.
[14] V. Kumar, C.K. Chang, K.P. Tan, Y.S. Jung, S.H. Chen, Y.S. Cheng, P.H. Liang, Identification, synthesis, and evaluation of new neuraminidase inhibitors, Org Lett, 16 (2014) 5060-5063.
[15] S.W. Kwok, J.R. Fotsing, R.J. Fraser, V.O. Rodionov, V.V. Fokin, Transition-metal-free catalytic synthesis of 1,5-diaryl-1,2,3-triazoles, Org Lett, 12 (2010) 4217-4219.
[16] S.H. Krake, P.D.G. Martinez, J. McLaren, E. Ryan, G. Chen, K. White, S.A. Charman, S. Campbell, P. Willis, L.C. Dias, Novel inhibitors of Plasmodium falciparum based on 2,5-disubstituted furans, Eur J Med Chem, 126 (2017) 929-936.
[17] G. Mulligan, C. Mitsiades, B. Bryant, F. Zhan, W.J. Chng, S. Roels, E. Koenig, A. Fergus, Y. Huang, P. Richardson, W.L. Trepicchio, A. Broyl, P. Sonneveld, J.D. Shaughnessy, Jr., P.L. Bergsagel, D. Schenkein, D.L. Esseltine, A. Boral, K.C. Anderson, Gene expression profiling and correlation with outcome in clinical trials of the proteasome inhibitor bortezomib, Blood, 109 (2007) 3177-3188.

[18] C.S. Sevier, C.A. Kaiser, Ero1 and redox homeostasis in the endoplasmic reticulum, Biochim Biophys Acta, 1783 (2008) 549-556.
[19] A. Tovchigrechko, I.A. Vakser, GRAMM-X public web server for protein-protein docking, Nucleic Acids Res, 34 (2006) W310-314.
[20] G.J. Yang, P.M. Lei, S.Y. Wong, D.L. Ma, C.H. Leung, Pharmacological Inhibition of LSD1 for Cancer Treatment, Molecules, 23 (2018).
[21] E. Lee, D.H. Lee, Emerging roles of protein disulfide isomerase in cancer, BMB Rep, 50 (2017) 401-410.

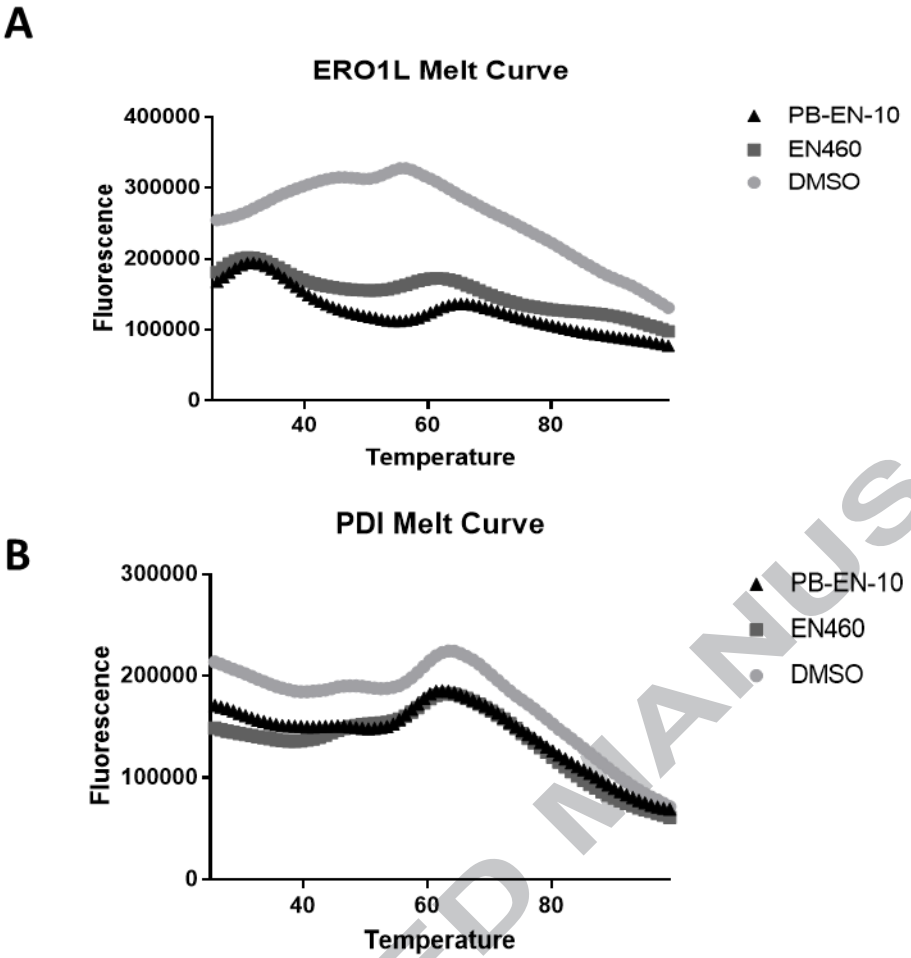

Supplemental Figure 1.

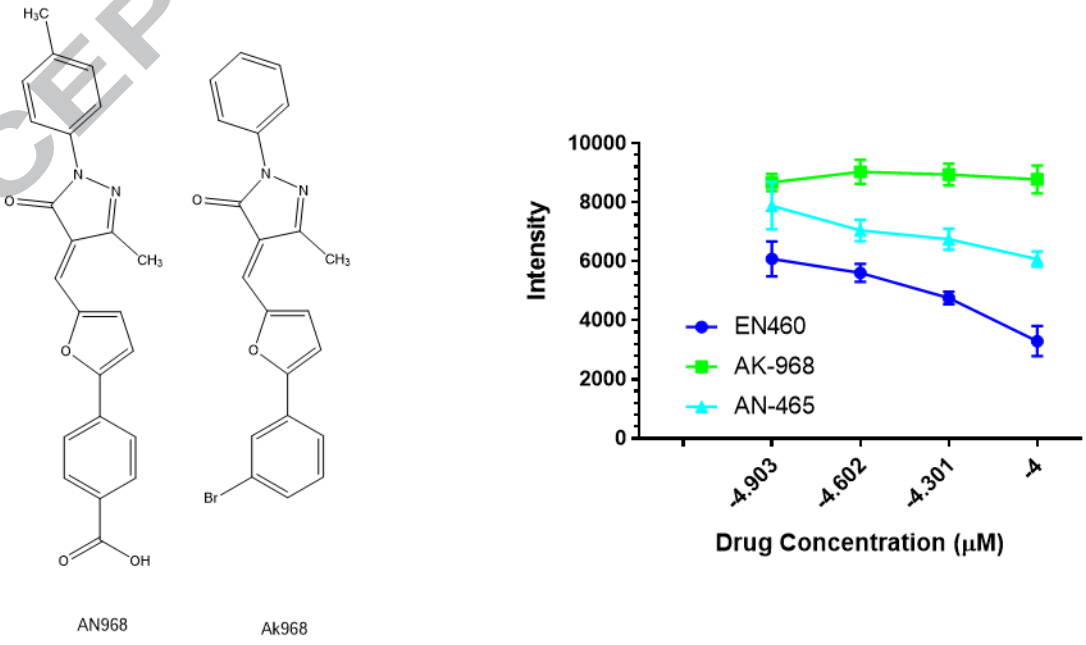

Supplemental Figure 2.